Deformation potentials of the $E_1(TO)$ and E_2 modes of InN

V. Darakchieva,[a] P. P. Paskov, E. Valcheva, T. Paskova, and B. Monemar
Department of Physics and Measurement Technology, Linköping University, S-581 83 Linköping, Sweden

M. Schubert
Fakultät für Physik and Geowissenschaften, Universität Leipzig, 04103 Leipzig, Germany

H. Lu and W. J. Schaff
Department of Electrical and Computer Engineering, Cornell University, Ithaca, New York 14853

(Received 5 January 2004; accepted 10 March 2004; published online 20 April 2004)

The deformation potentials of the $E_1(TO)$ and E_2 modes of InN are determined by combining infrared spectroscopic ellipsometry, Raman scattering, and x-ray diffraction measurements, and using a reported value of the mode Grüneisen parameter. The deformation potentials are obtained for two sets of stiffness constants. Strain-free values of the InN $E_1(TO)$ mode of 477.9 cm^{-1} and of the E_2 mode of 491.1 cm^{-1} have been determined. © *2004 American Institute of Physics.*
[DOI: 10.1063/1.1738520]

The group-III nitrides are currently a subject of intense investigations because of the substantial potential for applications for optoelectronic and high-speed devices in the ultraviolet, visible, and infrared energy region. InN is the least studied representative among the group-III nitrides due to difficulties to fabricate good-quality single-crystalline epitaxial films in the past thirty years. Recent progress in growth techniques allows the fabrication of higher crystalline quality hexagonal InN layers with relatively low electron concentration.[1] The group-III nitride layers are typically grown on foreign substrates, resulting in built-in strain in the films due to the difference in lattice parameters and thermal expansion coefficients between the epilayers and the substrates. IR and Raman spectroscopy are widely employed to probe the strain fields in heteroepitaxial AlN[2,3] and GaN,[4] since the phonon frequencies are directly related to a change of the chemical bond lengths. For this purpose, the phonon deformation potentials, which linearly relate the shift of the vibrational frequencies to the strain in the layers, are required. The deformation potentials of the zone-center optical phonons of GaN and AlN have been extensively studied,[2,4–8] whereas neither experimental nor theoretically calculated values of the phonon deformation potentials of InN are available.

In this work, the InN $E_1(TO)$ and E_2 deformation potentials are determined by combining x-ray diffraction, IR spectroscopic ellipsometry (IRSE), and Raman scattering studies of InN films with different thicknesses, and using the calculated Grüneisen parameter reported in Ref. 9. Correlations between strain and $E_1(TO)$ and E_2 frequencies also allow us to estimate the strain-free values of the respective mode frequencies.

We studied InN layers grown either on AlN or on GaN buffer layers on (0001) sapphire by molecular-beam epitaxy. The film thicknesses are in the range 200–1500 nm, details about the growth process and some structural and electrical characteristics have been published elsewhere.[1,10] Reciprocal space mapping and single $2\theta-\omega$ scans of the InN films were performed using a Philips X'pert MRD triple-axis diffractometer. All films studied exhibit a single-crystalline hexagonal structure with their c-axes parallel to the sapphire [0001] axis. No tetragonal metal In phase was detected. One representative map around the asymmetric $10\bar{1}5$ reciprocal space point is shown in the inset of Fig. 1. The narrow peak linewidths and the absence of diffuse scattering demonstrate a high crystal quality of the films. The c lattice parameter was determined from the symmetric $000\bar{2}$, $000\bar{4}$, and $000\bar{6}$ Bragg peaks. The asymmetric $10\bar{1}4$, $10\bar{1}5$, $20\bar{2}4$, and $20\bar{2}5$ reflections and the c lattice parameter were used for the determination of the a lattice parameter. The c and a lattice parameters of the films were calculated taking the refraction correction into account.[11] The achieved precision in the determination of the lattice parameters is 2×10^{-5} and 1×10^{-4} for the c and a lattice parameters, respectively. The

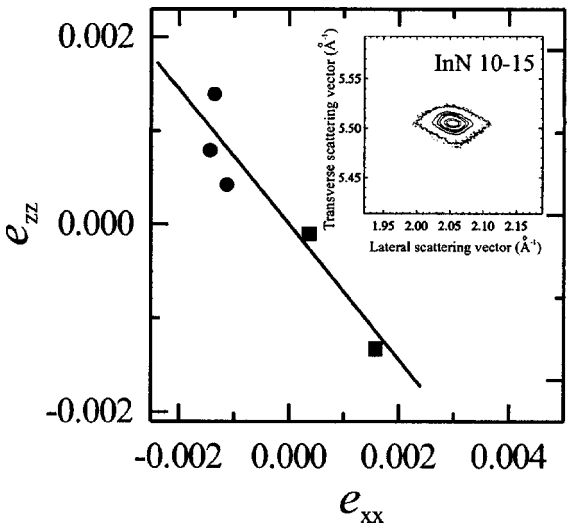

FIG. 1. Correlation between out-of-plane (e_{zz}) and in-plane (e_{xx}) strain for the InN samples studied (squares: samples on AlN buffer layer, dots: samples on GaN buffer layer). A representative reciprocal space map around the InN $10\bar{1}5$ Bragg peak of a 1500-nm-thick InN film is shown in the inset.

[a]Author to whom correspondence should be addressed; Electronic mail: vanya@ifm.liu.se

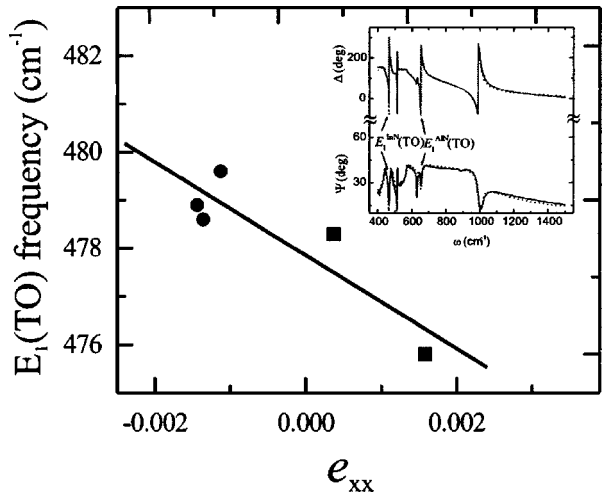

FIG. 2. E_1(TO) frequency versus the in-plane strain e_{xx} (squares: samples on AlN buffer layer, dots: samples on GaN buffer layer). The inset shows the experimental (dotted lines) and calculated (solid lines) IRSE Ψ and Δ spectra of one representative InN sample grown on an AlN buffer layer. The resonance features in the spectra due to InN E_1(TO) and AlN E_1(TO) modes are marked by arrows.

in-plane (e_{xx}) and out-of-plane (e_{zz}) strain in the samples are calculated using the following values for unstrained lattice parameters $c_0=5.7033$ Å and $a_0=3.5378$ Å (Ref. 12):

$$e_{xx}=(a-a_0)/a_0, \tag{1}$$

$$e_{zz}=(c-c_0)/c_0. \tag{2}$$

The correlation between the out-of-plane and in-plane strain for the samples studied is shown in Fig. 1. It is seen that two of the samples (grown on AlN buffer layers) experience tensile in-plane strain, while the rest (grown using GaN buffer layers) are compressively strained, similarly to previous observations.[13] The two strain components couple linearly as seen from Fig. 1 and, in the case of biaxial strain, the linear correlation between them is given via the stiffness constants, C_{ij}:

$$e_{zz}=-\frac{2C_{13}}{C_{33}}e_{xx}. \tag{3}$$

A linear fit to the experimental points in Fig. 1 gives a value of 0.72 for the $2C_{13}/C_{33}$, which is in very good agreement with the theoretical predictions of 0.68/0.755 (Ref. 14) as well as with an experimental value of 0.6, previously determined (Ref. 13). We note, however, that this ratio is sensitive to the uncertainties of stiffness constant values as well as to the values of the strain-free lattice parameters for the theoretical and experimental determinations, respectively.

Room-temperature IRSE measurements were performed in the spectral range 350–1500 cm^{-1}, with spectral resolution of 2 cm^{-1} and at 60° and 70° angles of incidence. The IRSE data were analyzed by employing anisotropic dielectric functions of InN, GaN, and AlN layers in the model calculations. Contributions from both the IR active polar phonons and the free carriers to the dielectric response of InN and GaN are accounted for, while only the phonon contribution to the AlN model dielectric function is considered. Details about the modeling and the regression analysis can be found in Ref. 15. The experimental and the best-fit IRSE Ψ and Δ spectra are shown in the inset of Fig. 2 for one representative sample grown on an AlN buffer layer. The IRSE spectra of the film provide a high sensitivity to the frequency and broadening parameter of the E_1(TO) mode. It is seen from Fig. 2 that a distinct spectral feature in Ψ and Δ appears near the InN E_1(TO) resonance. The frequency of the InN E_1(TO) mode is extracted from the best fits to the experimental IRSE spectra for all samples with an accuracy of 0.2–0.5 cm^{-1}. The E_1(TO) broadening parameter has a value between 2 and 4 cm^{-1} depending on the sample, in agreement with the x-ray results about the high crystal quality of the films. The determined E_1(TO) frequencies are plotted as function of the in-plane strain in the films in Fig. 2. The shift of the E_1(TO) frequency $\Delta\omega_{E_1(\mathrm{TO})}$ under strain is given by[16]

$$\Delta\omega_{E_1(\mathrm{TO})}=2a_{E_1(\mathrm{TO})}e_{xx}+b_{E_1(\mathrm{TO})}e_{zz}, \tag{4}$$

where $a_{E_1(\mathrm{TO})}$ and $b_{E_1(\mathrm{TO})}$ are the deformation potentials of the InN E_1(TO) mode. Using Eq. (3) and the results from Fig. 1, we obtain

$$\Delta\omega_{E_1(\mathrm{TO})}=(2a_{E_1(\mathrm{TO})}-0.72b_{E_1(\mathrm{TO})})e_{xx}. \tag{5}$$

The intersection of the linear fit to the experimental points in Fig. 2 with the zero strain gives a value of 477.9 cm^{-1} for the strain-free E_1(TO) frequency. Using the slope of the linear fit and the relation between the strain and the E_1(TO) frequency [Eq. (5)], we are able to determine a linear combination of the two deformation potentials. One more relation is needed for the determination of the deformation potentials $a_{E_1(\mathrm{TO})}$ and $b_{E_1(\mathrm{TO})}$. It can be obtained if the linear pressure coefficient of the mode is known. For hydrostatic pressure the diagonal components of the stress tensor are equal: $\sigma_{xx}=\sigma_{yy}=\sigma_{zz}=\sigma$. Therefore, the shift of the E_1(TO) frequency $\Delta\omega_{E_1(\mathrm{TO})}$ and the linear pressure coefficient $\partial\omega/\partial P$ are given by

$$\Delta\omega_{E_1(\mathrm{TO})}=\frac{\partial\omega}{\partial P}\sigma, \tag{6}$$

with

$$-\frac{\partial\omega}{\partial P}=2a_{E_1(\mathrm{TO})}(S_{11}+S_{12}+S_{13})+b_{E_1(\mathrm{TO})}(2S_{13}+S_{33}), \tag{7}$$

where S_{ij} are the compliance constants.

We found in the literature only one calculated value of the Grüneisen parameter of the InN E_1(TO) mode,[9] which is related to the linear pressure coefficient via $\gamma=(\partial\omega/\partial P)\times(B/\omega_0)$, where B is the bulk modulus, and ω_0 is the strain-free E_1(TO) frequency. In this way, the deformation potentials can be obtained from our experimental results and the Grüneisen parameter of the E_1(TO) mode[9] using Eqs. (5) and (7).

We also measured Raman scattering from the samples with 488 nm excitation and a spectral resolution of 1 cm^{-1}. The experiment was conducted in backscattering $z(x,-)\bar{z}$ configuration, with the film c axis parallel to the z direction. The allowed E_2 mode is detected in all samples (one representative Raman spectrum shown in the inset of Fig. 3). The extracted E_2 frequencies for all samples studied are plotted versus the in-plane strain e_{xx} in Fig. 3. A value of 491.1

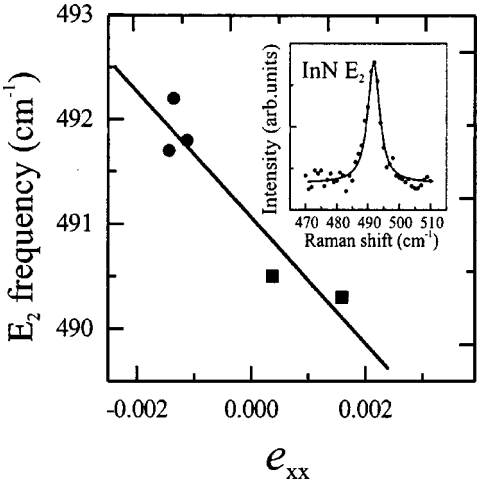

FIG. 3. E_2 frequency versus the in-plane strain e_{xx} (squares: samples on AlN buffer layer, dots: samples on GaN buffer layer). A representative Raman spectrum is shown in the inset.

cm^{-1} for the E_2 strain-free frequency is determined from the linear fit to the experimental points. Analogously to the E_1(TO) mode, the deformation potentials of the E_2 mode are then obtained.

Our previous study on E_1(TO) mode of AlN showed that the deformation potentials are very sensitive to the elastic constants values.[2] Therefore, we calculated the deformation potentials of the E_1(TO) and E_2 modes of InN for two sets of elastic constants.[9,17] The compliance tensor $\hat{S}$ was obtained by numerical inversion of the stiffness tensor $\hat{C}$ for each set of C_{ij}. The obtained values are summarized in Table I.

Similarly to GaN and AlN,[2,4,5,7,8] the deformation potentials of both E_1(TO) and E_2 modes of InN are negative (Table I). The values of the deformation potentials of InN are expected to be smaller than the respective deformation potentials of GaN due to the weaker bonding in InN.[7] We compared our values of the deformation potentials of InN with the respective experimental deformation potentials of GaN reported by Davydov *et al.*[4] and Demangeot *et al.*[5] We found that all values in Table I fulfill the aforementioned relation being smaller than the respective deformation potentials of GaN. The lack of any other theoretical and experimental values of the InN deformation potentials prevents any comparative analysis on the two sets of deformation potentials. We also note that the as determined deformation potentials depend not only on the stiffness constants, but also on the mode Grüneisen parameter.[2] No experimental value for the latter is available.

TABLE I. Deformation potentials a and b of the InN E_1(TO) and E_2 modes obtained using different values of the elastic stiffness tensor elements C_{ij}.

C_{ij}	$a_{E_1(\mathrm{TO})}$ (cm^{-1})	$b_{E_1(\mathrm{TO})}$ (cm^{-1})	a_{E_2} (cm^{-1})	b_{E_2} (cm^{-1})
Ref. 9	−735	−699	−610	−857
Ref. 17	−715	−644	−611	−861

It is worth mentioning that the strain-free frequencies of E_1(TO) and E_2 modes determined in this work are very close to the theoretical predictions of Bechstedt *et al.*,[18] being slightly larger. The latter is not surprising since it is well known that the *ab initio* density-functional theory calculations used in Ref. 18 tend to give underestimated values.

In summary, we have determined the deformation potentials of InN E_1(TO) and E_2 modes for two different sets of stiffness constants to be: $a_{E_1(\mathrm{TO})}=-735$ cm^{-1} and $b_{E_1(\mathrm{TO})}=-699$ cm^{-1} ($a_{E_1(\mathrm{TO})}=-715$ cm^{-1} and $b_{E_1(\mathrm{TO})}=-644$ cm^{-1}) for the E_1(TO); and $a_{E_2}=-610$ cm^{-1} and $b_{E_2}=-857$ cm^{-1} ($a_{E_2}=-611$ cm^{-1} and $b_{E_2}=-861$ cm^{-1}) for the E_2, respectively. We have also estimated the strain-free frequencies of the E_1(TO) and E_2 modes to be 477.9 cm^{-1} and 491.1 cm^{-1}, respectively.

[1] H. Lu, W. J. Schaff, J. Hwang, H. Wu, G. Koley, and L. F. Eastman, Appl. Phys. Lett. **79**, 1489 (2001).
[2] V. Darakchieva, P. P. Paskov, T. Paskova, J. Birch, S. Tungasmita, and B. Monemar, Appl. Phys. Lett. **80**, 2302 (2002).
[3] T. Prokofyeva, M. Seon, J. Vanbuskrik, M. Holtz, S. A. Nikishin, N. N. Faleev, H. Temkin, and S. Zollner, Phys. Rev. B **63**, 125313 (2001).
[4] V. Yu. Davydov, N. S. Averkiev, I. N. Goncharuk, D. K. Nelson, I. P. Nikitina, A. S. Polkovnikov, A. N. Smirnov, M. A. Jacobson, and O. K. Semchinova, J. Appl. Phys. **82**, 5097 (1997).
[5] F. Demangeot, J. Frandon, M. A. Renucci, O. Briot, B. Gil, and R. L. Aulombard, Solid State Commun. **100**, 207 (1996).
[6] A. Sarua, M. Kuball, and J. E. Nostrand, Appl. Phys. Lett. **81**, 1426 (2002).
[7] J. M. Wagner and F. Bechstedt, Appl. Phys. Lett. **77**, 346 (2000).
[8] J. Gleize, M. A. Renucci, J. Frandon, E. Ballet-Amalric, and B. Daudin, J. Appl. Phys. **93**, 2065 (2003).
[9] K. Kim, W. L. Lambrecht, and B. Segall, Phys. Rev. B **53**, 16310 (1996).
[10] C. J. Lu, L. A. Bendersky, H. Lu, and W. J. Schaff, Appl. Phys. Lett. **83**, 2817 (2003).
[11] V. Darakchieva, P. P. Paskov, T. Paskova, E. Valcheva, B. Monemar, and M. Heuken, Appl. Phys. Lett. **82**, 703 (2003).
[12] W. Paszkowicz, Powder Diffr. **14**, 258 (1999).
[13] V. Cimalla, Ch. Förster, G. Kittler, I. Cimalla, R. Kosiba, G. Ecke, O. Ambaher, R. Goldhahn, S. Shokhovets, A. Georgakilas, H. Lu, and W. J. Schaff, Phys. Status Solidi C **0**, 2818 (2003).
[14] A. Zoroddu, F. Bernardini, P. Ruggerone, and V. Fiorentini, Phys. Rev. B **64**, 045208 (2001).
[15] M. Schubert, in *Infrared Ellipsometry on Semiconductor Layer Structures: Phonons, Plasmons and Polaritons* (Springer, Berlin, 2004).
[16] R. J. Briggs and A. K. Ramdas, Phys. Rev. B **13**, 5518 (1976).
[17] A. F. Wright, J. Appl. Phys. **82**, 2833 (1997).
[18] F. Bechstedt, U. Grossner, and J. Furthmüller, Phys. Rev. B **62**, 8003 (2000).